Liquid Crystal-Induced Myoblast Alignment

DOI: 10.1002/ ((please add manuscript number))
Article type: Full Paper

Liquid crystal-induced myoblast alignment

*Daniele Martella, Lorenzo Pattelli, Camilla Matassini, Francesca Ridi, Massimo Bonini, Paolo Paoli, Piero Baglioni, Diederik S. Wiersma, and Camilla Parmeggiani**

Dr. D. Martella, Dr. C. Matassini, Dr. F. Ridi, Prof. M. Bonini, Prof. P. Baglioni, Dr. C. Parmeggiani
Department of Chemistry "Ugo Schiff", University of Florence, via della Lastruccia 3-13 - 50019 Sesto Fiorentino, Italy
E-mail: camilla.parmeggiani@lens.unifi.it
Dr. D. Martella, Dr. L. Pattelli, Prof. D. S. Wiersma, Dr. C. Parmeggiani
European Laboratory for Non-linear Spectroscopy, via Nello Carrara 1 -50019 Sesto Fiorentino, Italy
Dr. D. Martella, Dr. C. Matassini, Dr. C Parmeggiani
National Institute of Optics, National Research Council, via Nello Carrara 1 -50019 Sesto Fiorentino, Italy
Dr. L. Pattelli, Prof. D. S. Wiersma
Department of Physics and Astronomy, University of Florence, Via Sansone, 1 - 50019 Sesto Fiorentino, Italy
Dr. L. Pattelli, Prof. D. S. Wiersma, Dr. C. Parmeggiani
Istituto Nazionale di Ricerca Metrologica INRiM, Strada delle Cacce, 91 - 10135 Turin, Italy
Dr. F. Ridi, Prof. M. Bonini, Prof. P. Baglioni
CSGI, Center for Colloids and Interface Science, via della Lastruccia, 3 - 50019 Sesto Fiorentino, Italy
Prof. P. Paoli
Department of Biochemical, Experimental and Clinical "Mario Serio", Viale Morgagni 50 Firenze, 50134, Italy

Keywords: liquid crystalline network, cell alignment, biomaterials, muscular tissue engineering, liquid crystalline alignments

The ability to control cell alignment represents a fundamental requirement towards the production of tissue *in vitro* but also to create bio-hybrid materials presenting the functional properties of human organs. However, cell cultures on standard commercial supports do not provide a selective control on the cell organization morphology, and different techniques, such as the use of patterned or stimulated substrates, have been developed to induce cellular alignment. In this work, a new approach towards *in vitro* muscular tissue morphogenesis is presented exploiting Liquid Crystalline Networks. By using smooth polymeric films with

planar homogeneous alignment, a certain degree of cellular order is observed in myoblast cultures with direction of higher cell alignment corresponding to the nematic director. The molecular organization inside the polymer determines such effect since no cell organization is observed using homeotropic or isotropic samples. These findings represent the first example of cellular alignment induced by the interaction with a nematic polymeric scaffold, setting the stage for new applications of liquid crystal polymers as active matter to control tissue growth.

1. Introduction

The ability to reproduce a correct morphogenesis *in vitro* is mandatory to engineer human tissues with the same characteristic of the targeted native one. For this reason, artificial methods to direct cellular proliferation and motility are the basis to properly restore, maintain, or improve damaged tissue functionality. Human tissues grow according to specific morphogenetic pathways in which the cell differentiation process drives the correct organism development in terms of shape and functionality. A crucial aspect for a correct morphogenesis of many tissues rely on the cell alignment, which is responsible for specific biological functions. For example, pulsatile flow of blood in blood vessels is provided by specific tensile strength and flexibility deriving from anisotropic cell organizations.[1] Analogously, development of muscular contractile forces, needed for the different body movements (from muscle contraction to heart beating), depends on the highly anisotropic myoblasts arrangement resulting in myotube-containing fibers, vital for muscle functionality.[2]

Strong efforts were done in recent years to develop biological or synthetic substitutes for tissue reconstruction[3] and a variety of approaches emerged to reproduce natural cell alignment including mechanical loading, topographical patterning and surface chemical treatment.[4] Most of the already reported polymeric scaffolds are based on 2D systems and use simple topographical features such as grooves or pillar to direct cell growth.[5]

On the other hand, current physiological and biophysical studies are recognizing the possibility to describe a variety of biological tissues as active liquid crystals (LC), in which cell growth, alignment and migration can be described according to models developed for theses anisotropic phases.[6] A common feature of liquid crystalline molecules, both synthetic and biological, is an anisotropic (generally rod-like) shape which is responsible for the anisotropy of different system properties. Using 2D cell cultures, it was observed as spindle shaped cells, such as fibroblasts and neuroblasts, at high density are able to form ordered domains of some tens of cells. During their proliferation, neighboring cells interact with each other and the collective dynamics of their assembly evolves toward a progressive ordered arrangement up to reach a high density nematic state.[7] More interestingly, *in vitro* studies have also demonstrated that the formation of topological singularities and of collective cell patterns (both following nematic models) are phenomena driving cellular functions such as epithelial cell extrusion from a tissue.[8] In this regard, an exciting possibility is to directly translate the organization of the synthetic liquid crystal into a cell culture, therefore enabling the control of cell growth through molecular engineering of the polymers. This concept was already demonstrated for self-propelled bacteria, showing how to transform their chaotic motion into a controlled swimming thanks to their dispersion in a lyotropic LC environment. Such elegant example highlights the possibility to manipulate biological elements by means of materials with anisotropic composition translating an “information” contained at molecular level in the scaffold into a living system.[9]

However, the extension of the same concept to cell cultures is not trivial. One of the main issues in this regard is the need of scaffolds with well-defined mechanical properties, able to mimic the natural extracellular environment. Standard LCs lack this characteristic, thus preventing cell adhesion. The first example of fibroblast culture on LC materials was reported by using a nematic fluid consisting of a colloidal network of polystyrene beads with sufficient bulk elasticity (in the kPa range) to support cell adhesion.[10] However, this approach failed

for other cell lines that require more rigid substrates. This problem was recently solved by the introduction of liquid crystalline networks (LCN) as cell scaffolds.[11] These materials can be elastomers or thermosets exhibiting mechanical elasticity ranging from MPa to GPa,[12] and have been extensively studied as smart shape-changing materials.[13] In fact, they are able to undergo reversible shape-change thanks to the liquid crystalline to isotropic phase transition of the mesogens. [14] Such deformations can be triggered by many different stimuli[13] opening to applications which range from soft robotics (from macroscopic motors to microdevices)[15] to photonic devices.[16]

To date, adhesion and growth of different cell lines, from neuroblastoma[17] to cardiomyocyte, were demonstrated on LCN presenting different chemical structures such as polysiloxane[18] or polyester[19] based LC polymers. More recently, we have demonstrated acrylate-based LCNs, prepared through a quick and clean synthetic route from commercial monomers, to be versatile supports for different cell lines.[20] Aligned regions were spontaneously formed in both fibroblast and myoblast cultures, while stem-cell derived cardiomyocyte grew with elongated anisotropic shape showing a mature adult-like shape and behavior.[20] Such alignment was demonstrated to be affected by the material rigidity but no evidence of a correlation with the molecular alignment was highlighted. Similar acrylate-based LCNs have also been reported to harness migration of fibroblast by means of light irradiation.[21]

This paper for the first time demonstrates the interplay between molecular and cell alignments, reporting a detailed study on the relationship between myoblast spontaneous alignment on acrylate LCNs and the characteristics of the material (focusing on fabrication protocol and LC alignment) to understand if it is possible to manipulate cell organization without using more complex techniques such as surface treatment/patterning. Myoblasts were selected because loss of muscle contractility occurs in different life-threatening diseases that can be currently only barely restored by medical and surgical treatments, therefore calling for the development of biological or synthetic substitutes for muscular reconstruction.[3] Achieving an aligned

myoblast organization represents an essential requirement towards growth of human muscular tissues *in vitro* and the capability to control it simply by the "nature" of the material (without the needing of post-functionalization or structuration) would be of great interest towards a real application in muscle tissue engineering. In this respect, the experiment reported here represents a step towards the large-scale control of myoblast alignment.

2. Results and Discussion

To test the effect of liquid crystalline scaffolds on the behavior of muscle cells, we investigated the common and commercially available C2C12 murine myoblasts cell culture. This choice was driven by the high medical interest towards replicating muscle morphogenesis and the common use of the selected cell line as skeletal muscle models.[22]

Using standard Petri dishes as scaffold, a chaotic cell growth was observed, without any trace of collective self-organization or a global cell alignment (**Figure 1**). A statistical analysis of the cell alignment confirms the absence of a preferential orientation of the nuclei (Figure 1). This result is very far from reproducing myoblast growth in their native environment, and calls for the development of different supports to assist the correct cell alignment.[23]

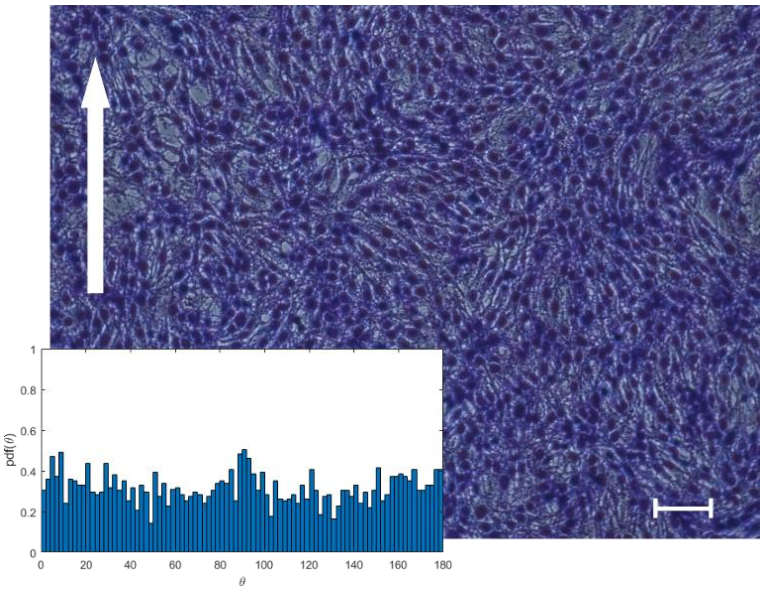

Figure 1. A chaotic myoblast culture on a standard Petri Dish. Optical image and directionality histogram showing the probability density function to find a cell tilted by a certain angle θ with respect to a reference 0° angle (white arrow). Scale bar: 100 μm.

The materials here used as cell scaffold are Liquid Crystalline Network (LNC) prepared by photopolymerization of acrylate groups[24] after alignment of the monomeric materials in standard LC cells. In particular, the compounds used in this study are reported in **Figure 2**. Molecules **1** and **2** are commercial polymerizable mesogens that allows for the formation of LC polymers and the easy modulation of the final polymer properties. Previous studies demonstrated how, by adjusting the ratio between the monoacrylate **1** and the crosslinker **2**, it is possible to obtain different mechanical stiffness[25] or to influence the resolution during the 3D photolithographic processes.[26] Molecule **3** (Irgacure 369) was used as photoinitiator.

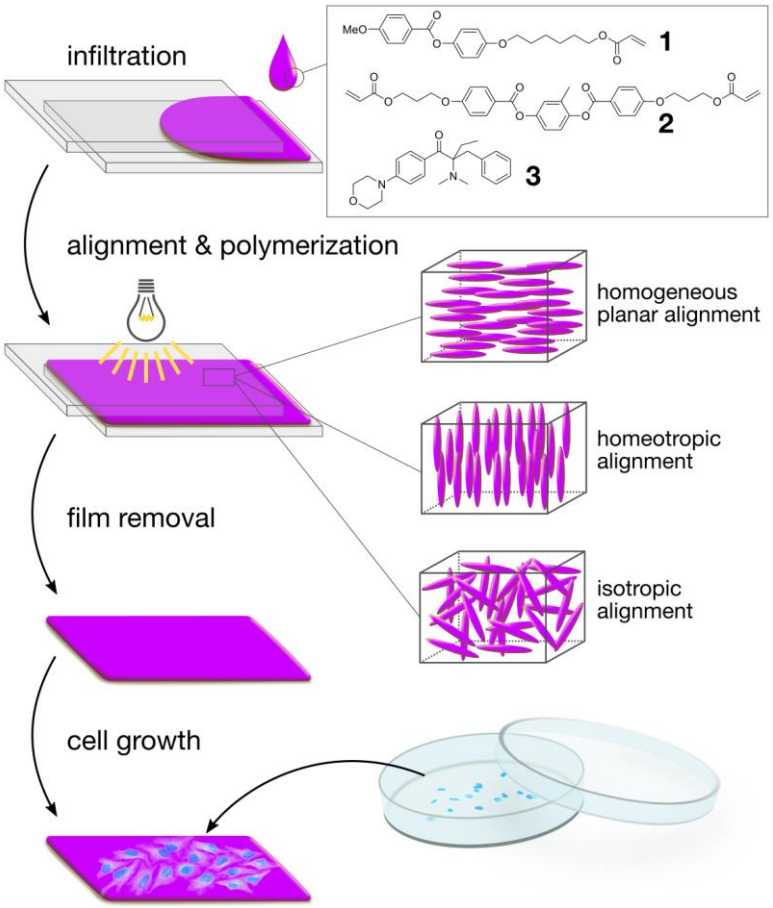

Figure 2. Scheme of material fabrication and molecular structure of the monomeric compounds.

Using films made by the same molecules, we recently reported how different cell lines are able to adhere and grow on the substrate without the need of any particular surface treatment

or coating. Interestingly, during cell proliferation, a spontaneous cell alignment was observed for both myoblast and fibroblast cultures at high density, highlighting a dependence from material composition (e.g. amount of crosslinker).[20] On the basis of this previous analysis, we performed most of the experiments using films containing 20% mol/mol of the crosslinker, but presenting different molecular alignments. In particular, we prepared materials polymerized starting from the nematic phase (oriented in a planar homogeneous or homeotropic way) or from the isotropic phase of the monomers. A scheme of the performed experiments is reported in Figure 2.

The monomeric mixture was melted, infiltrated by capillaries in different liquid crystalline cells (depending on the desired alignment), cooled down to the nematic phase, and polymerized by a UV lamp (Figure 2). Samples obtained from the isotropic phase were polymerized at 90 °C after infiltration by the use of two different kind of glass cells (one made by untreated glasses and the other using the same rubbed cell described for the obtainment of the planar homogeneous alignment). The high polymerization temperature ensures the obtainment of isotropic films, while the use of the rubbed cell would allow to detect possible surface topography effects to drive the cellular alignment. The selected synthetic strategy (free radical polymerization) allows to obtain the material in one quick step (by simultaneous growth of the polymeric chains and their crosslinking) and to retain the LC alignment inside the final material. Planar homogeneous and isotropic samples were characterized by different microscopic techniques, to have insight about their surface morphology, and by tensiometric measurements. All tests were carried out after a sterilization protocol (required by the following biological studies) to be sure that the analyzed surfaces were as similar as possible to those used as cell scaffolds. In all cases, no evidence of microstructuration is present on the surfaces as shown by representative SEM images reported in **Figure 3** (a, c, e). A small amount of inhomogeneity (without any anisotropic arrangement) are present on the surface of samples prepared in the polyvinyl alcohol (PVA) rubbed cells.

To further elucidate this point, we investigated the same samples by atomic force microscopy. AFM micrographs at different magnifications are reported in Figure 3 (b, d, f), with the direction of rubbing (when applied) aligned vertically. The surface morphology at the nanoscale does not show a defined order and also in this case no evidence of anisotropic structuration is observed in any sample. The AFM micrographs were also used to evaluate the roughness of the films (see Experimental part) and are reported in Figure 3g.

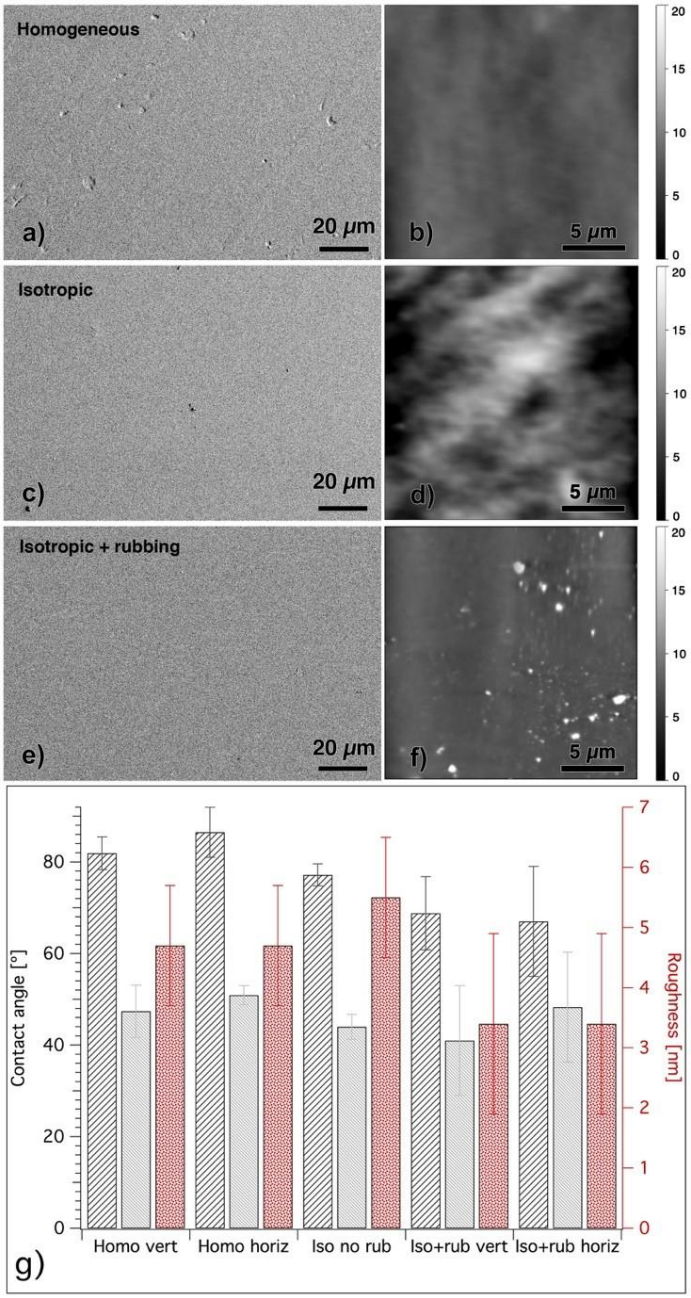

Figure 3. Material surface characterization. SEM (left, a, c, e) and AFM (right, b, d, f) micrographs of homogeneous, isotropic and isotropic (made in the rubbed cell) samples. g) Advancing and receding contact angle (grey bars) and roughness value (red bars, right y-axis)

of the analyzed samples: the rubbed samples were investigated in vertical and horizontal directions.

These analyses did not show significant differences between the samples, suggesting that the use of a rubbed coating in the polymerization cells does not significantly modify the material surface morphology.

The films were also characterized in terms of their wettability, as this could affect the growth of cells. In particular, we evaluated if the rubbing process results in different wettability along or perpendicularly to the rubbing direction. The results are given in Figure 3g, in terms of the advancing/receding contact angle when the film is vertically immersed/removed in water. Also in this case, no dramatic differences were found. In particular, the rubbing process does not seem to affect the wettability properties neither of the planar homogeneous sample nor of the isotropic rubbed sample, indeed they both show very similar values to those of the isotropic samples.

After such physico-chemical characterization, the materials were directly employed for the myoblast culture without further purification process or surface treatment. Stripes with dimensions around 10 mm x 3 mm were cut with longer dimension corresponding to the rubbing direction (if present). After sterilization, C2C12 myoblasts were seeded directly on the LCNs and the samples were incubated in standard conditions.

The biological assays were stopped after 72 hours of incubation and LCNs were washed with Phosphate Buffered Saline (PBS), necessary to remove non-adherent cells; then they were stained with haematoxylin and eosin solutions. The samples were analyzed by optical microscopy and representative pictures of the C2C12 culture are reported in **Figure 4**. In all cases, we observed high cellular density, with cells presenting around 90% of confluence. A first evaluation by optical microscopy demonstrated that, depending on the chosen LC alignment, cells behave differently. For homogeneous planar films, a global cell orientation was observed with the preferential alignment direction of the nucleus nearly corresponding to

the LC director, highlighting how such molecular parameter can influence the myoblast orientation. In fact, this anisotropic organization is present only in the planar homogeneous samples, while chaotic cell alignment is observed in all the other substrates.

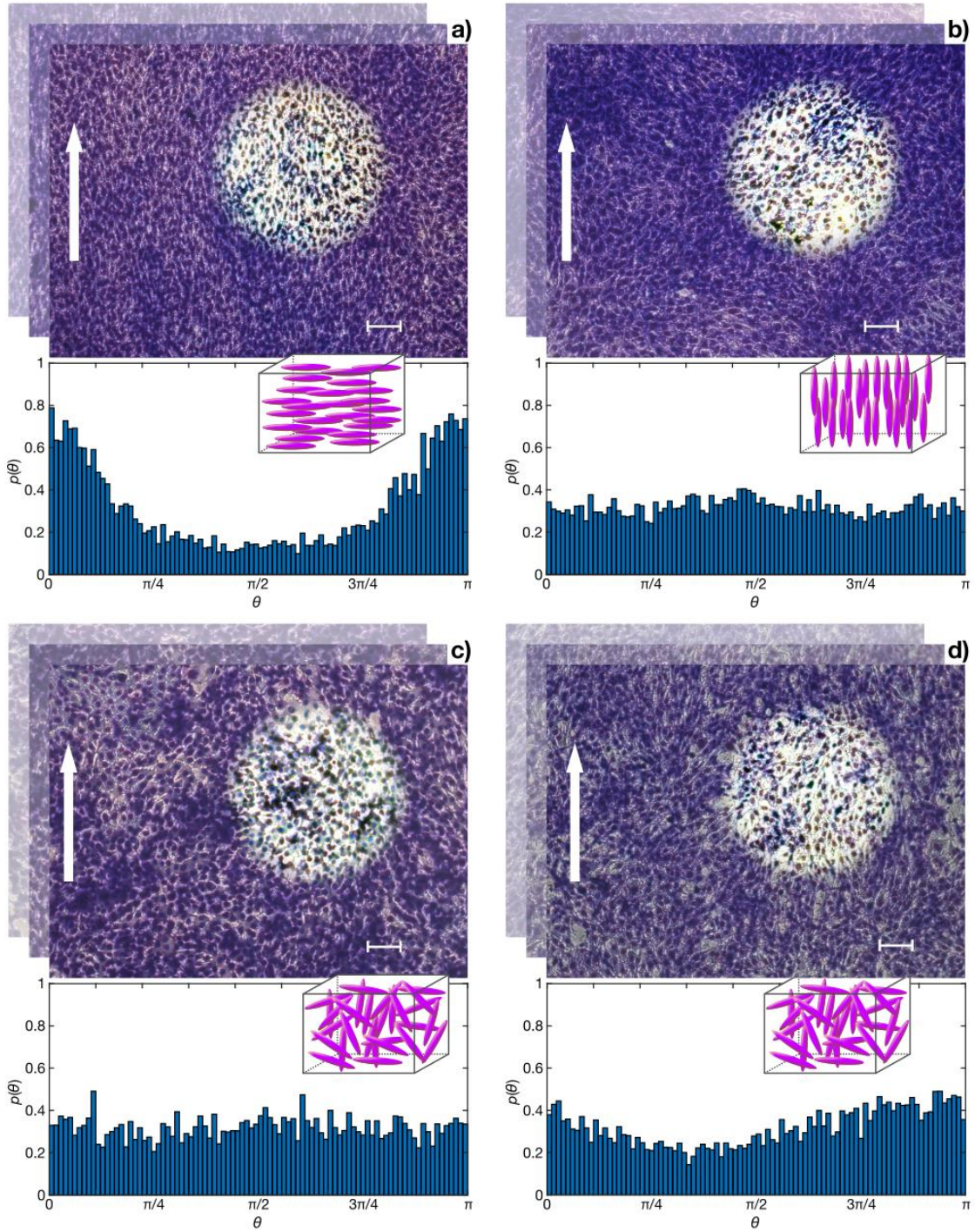

Figure 4. C2C12 culture on LCNs with different alignments. Each panel shows representative optical images (top) and directionality histogram (bottom) for cells grown on a) homogeneous planar sample, b) homeotropic sample, c) isotropic sample (polymerized in an untreated cell) and d) isotropic sample (polymerized in a PVA rubbed cell). The degree of cell alignment is highlighted for each sample by enhancing the contrast in a region of the illustrative image.

The histograms report the probability density function to find a cell tilted by a certain angle θ with respect to a reference 0° angle (white arrow). Scale bar: 100 μm.

For each sample, we quantitatively estimated the cellular alignment by performing a statistical analysis on ensembles of ~10^4 cells, combining images taken at different positions on different substrate (see Experimental Part and **Figures S1** and **S2**). Considering the ellipsoidal shape of the nucleus, it is possible to determine the tilting angle with respect to a reference direction (considering the nucleus major axis as cell orientation direction). The resulting directionality histograms are plotted in Figure 4 and report the probability density function to find a cell tilted with respect to a reference 0° angle (indicated by the white arrow). For rubbed samples, such direction also corresponds to the rubbing one. The statistical analysis confirmed the stark effect of liquid crystal alignment on cell orientation.

For a more quantitative comparison between the samples, we calculated from the directional plots both the order parameter (S) of myoblasts and their fraction (f) falling within 10 or 20 degrees from the preferential alignment direction (which, depending on how precisely the film strips have been cut, might be slightly different from the 0° direction).

The order parameter (S) was calculated by adjusting the standard formula used for liquid crystal models, according to Landau-de Gennes theory,[27] for the two dimensional case of adherent cells growth on a flat support. For 2D system, the order parameter can be obtained by **Equation 1**:[28]

$$S = \langle 2\cos^2\theta - 1 \rangle \qquad (1)$$

where θ describes the angle between the major axis of the elongated cell nuclei and the longer stripe side (which corresponds also to the nematic director if present).

In the limiting cases, a completely disordered state gives a value of S around 0 and, a perfect nematic order, where all the cells align with their neighbors, gives a value of S = 1.

For the planar homogenous sample, we found values of S = 0.35(7) and f = 25% and 46% for intervals of 10 and 20 degrees half-width ranges, respectively. Performing the same analysis on the homeotropic and isotropic samples with respect to the 0° direction we obtained values of S = -0.03(5) and S = -0.01(3), while the fractions of aligned cells are f = 11% and 12% (within 10 degrees) and f = 22% and 24% (within 20 degrees) respectively, confirming the absence of a preferred alignment. In the case of the film polymerized in the rubbed cell, we found a very small degree of cellular alignment which resulted in S = 0.17(4) and f = 17% and 37% for intervals of 10 and 20 degrees half-width ranges centered on the direction of preferential alignment (occurring around -23°). It is possible that a very low degree of molecular alignment of the molecules in touch with the rubbed glass is still present, also if polymerization occurs in the isotropic phase, and that cells are able to detect and be influenced by it. This would justify the different behavior of the isotropic samples polymerized in different conditions, since no topographical differences were highlighted by the SEM and AFM images (Figure 3). This result demonstrates how controlling the liquid crystalline alignment is required to obtain a significant degree of aligned cells for this kind of polymeric scaffolds. Thus, the smooth polymeric film with engineered LC order is able to assist the collective behavior of packed cells driving their unidirectional alignment. The comparison of our results with the strategies already described to align different kind of cells could help clarifying the observed behavior. In fact, while topographical patterning in the micrometric scale is the most widely explored strategy to force cell growth with a fixed alignment, especially for muscular cells,[5,29] in our case, no anisotropic microstructuration is present on the surfaces suggesting that other factors drive the cell alignment. A significant difference between the microstructuring alignment mechanism and our study is that, while the former method operates at a single cell level during their growth to form a well aligned culture, optical image of C2C12 culture on homogeneous sample at lower confluence shows that cell alignment is not present (**Figure S3**). This observation suggests that the C2C12

spontaneous alignment arises during cell bundles formation and the material affects mostly the collective behavior of such cell nuclei assembly nuclei rather than single cells. After seeding, the cells adhere to the substrate with casual orientation and during their proliferation, small clusters of aligned nuclei start to form even if a global alignment direction is not observed as demonstrated in Figure S3. Only as density increases due to proliferation, neighboring cells start to exhibit a collective orientation and the whole system evolves progressively from the initial disordered state into a high density anisotropic arrangement. The behavior is analogous to that observed in case of long-range orientational order formation for fibroblasts growth in channel-like confinements,[30] in which alignment of cell bundles was described by encapsulation of cells in high aspect ratio rectangular constructs. In this case, due to geometric effects and wall construct of the support, cells at high density result aligned with a preferential direction along the longer wall of the construct.[31] In our samples, geometric effects, possibly induced by the film border, play only a small role. As shown in **Figure S4** for a homeotropic sample, it is indeed possible to observe (in selected parts of the film) few aligned cells along the film border. Such effect propagates to neighboring cells for a limited extent, and in any case for not more than 4 lines of aligned C2C12 cells, but it is not translated to the bulk culture. Therefore, topographic features at the nanoscale can influence cell growth[32] but also in this case, the non anisotropic nature of our material surface at the nanoscale suggests that the main reason of cell alignment has to be found elsewhere.

Excluding all these surface aligning effects, the nature of the anisotropic culture in homogeneous film can be ascribed only to the molecular nematic organization. For planar homogeneous samples mechanical properties are anisotropic,[33] possibly influencing the cell movement and providing anisotropic friction between cells and the substrate. On the other hand, also the different interaction between the different chemical groups exposed on the extracellular matrices with the anisotropically arranged LC molecules could give rise to

anisotropic interaction. Clarifying uniquely the mechanism beyond the liquid crystal-assisted alignment of myoblast culture is not trivial: many effects and parameters should be evaluated and even a complete analysis of them could maybe give an exhaustive explanation of the results. However, our experiments clearly highlight the correlation between molecular and cellular alignment. To further expand the liquid crystal-induced cell alignment demonstration, different material processing and chemical compositions were evaluated (**Figure 5**).

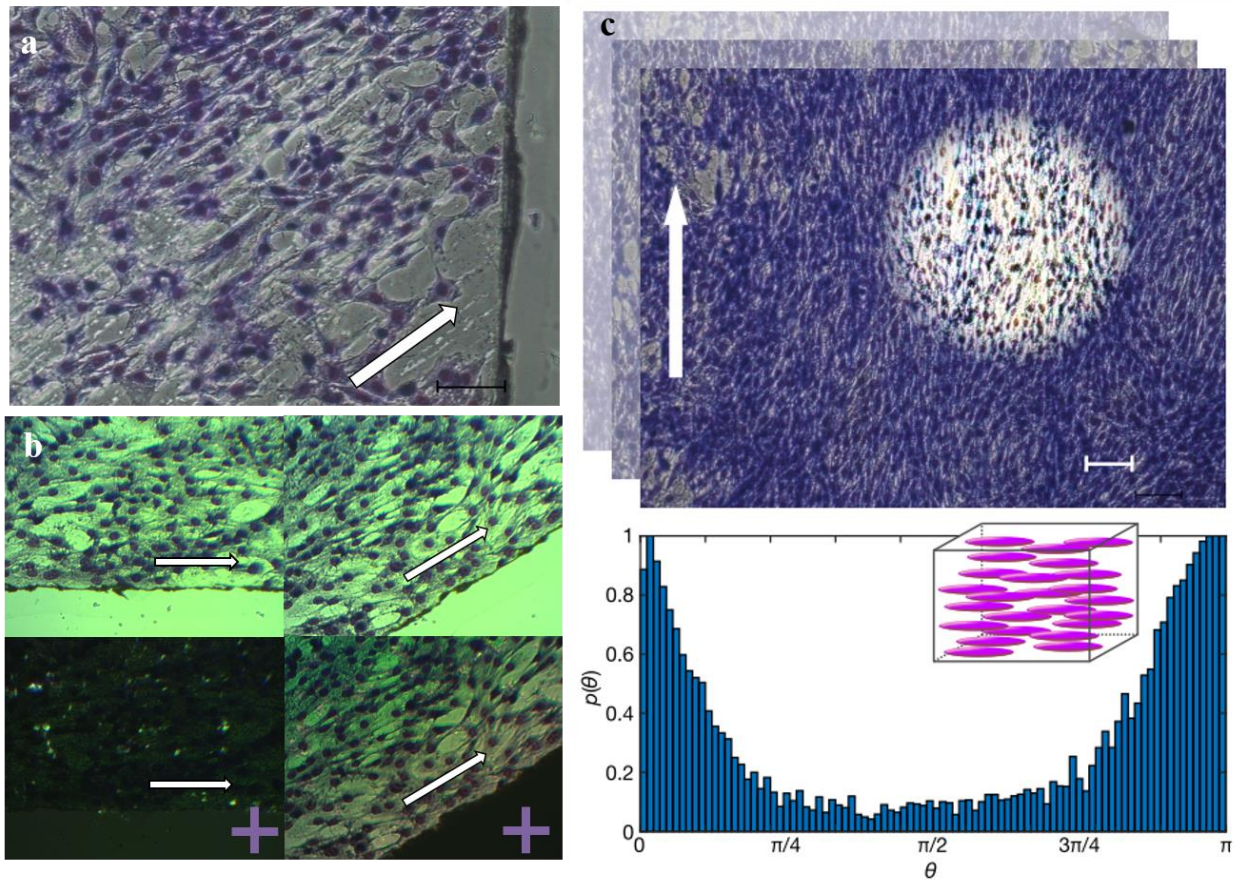

Figure 5. Extending the scope of liquid crystal-assisted myoblast alignment. a) C2C12 cultured on a homogeneous planar LCN stripe cut at 45° with respect to the nematic director. Scale bar: 100 µm b) Optical images by unpolarized (top) and polarized (bottom) light of a C2C12 culture on LCN. For planar homogeneous LC, the transmittance extinction by sample rotation of 45° can be used to check the molecular alignment quality. White arrows indicate the nematic director, while the purple cross show the cross polarizers. c) Representative optical image (top, scale bar: 100 µm) and directionality histogram (bottom) for C2C12 culture on planar homogeneous LCN with higher amount of crosslinker (40% mol/mol). The histogram reports the probability density function to find a cell tilted by a certain angle θ with respect to a reference 0° angle (white arrow).

As a first test, the planar homogeneous films were cut in rectangular stripes at 45° with respect to the nematic director. Also in this case the cellular alignment follows the nematic director and aligned cells result tilted with respect to the film border (Figure 5a). Cutting LCN materials at different angles with respect to the director can also result in helicoidally and curled structures[34] used to obtain 3D complex out-of-plane deformations. This effect could be coupled with the liquid crystal-assisted cell alignment opening to complex 3D scaffolds able to drive cell alignment and even bio-hybrid robots. The preferential cell alignment direction obtained by choosing the molecular alignment of the material can be easily checked by Polarized Optical Microscopy (POM), as shown in Figure 5b which reveals a defect-free monodomain texture. Moreover, playing on material composition could result in a different interplay between LC order and cell alignment, which depends on a complex process involving both the strength of cell-cell and cell-scaffold interactions. We already reported that increasing the amount of crosslinker in the films (from 10% to 20% mol/mol), leads to higher elastic modulus and thus to a different cell behavior, being greatly dependent on material rigidity.[20] Following these previous results, we also evaluated planar homogeneous films prepared by changing the molecular composition and, in particular, using 40 % mol/mol of diacrylate CL1 and 59 %mol/mol of M1. This chemical modification leads to a strong decrease of the polymer elastic behavior, with elastic modulus changing up to one order of magnitude by modifying the crosslinker percentage from 20 to 40, and storage modulus values around 15 and 130 MPa for similar samples (same mixture with addition of 1% of an azodye) at 37 °C.[25] Differential Scanning Calorimetry also confirms that thermal properties of the two formulations are very different, with glass transition temperatures of 30 °C and 54 °C respectively for the sample with 20% and 40% of crosslinker (see **Figure S5** for DSC traces). This indicates that, in the cell culture conditions, the first material is in its rubbery state while the second one is in its glassy state. On the other hand, investigation by polarized absorption spectroscopy (reported in **Figure S6**) reveals that the LC order parameter of the

two films is very similar, with values of 0.49 and 0.52 for the LCN samples containing 20% and 40% of crosslinker, respectively. Thus, increasing the quantity of diacrylate compound leads only to small increase of the overall nematic order. A C2C12 culture was performed on the new homogeneous planar sample showing that, also in this case, the liquid crystal-assisted alignment takes place with myoblast preferentially aligned along the nematic director. Very interestingly, the orientational graph reported in Figure 5c highlighted an even more pronounced ability of the material to guide the cell organization, with 2D cell order parameter reaching a value of S= 0.58(9), significantly higher than the value found for the material with 20% of cross-linker (S=0.35). Similarly, the fraction of cells aligned within 10 or 20 degrees from the preferential alignment direction is equal to 56% and 81%, respectively. These results clearly highlight how there are many factors, all dependent on typical LC phases anisotropy, playing a role on the ability of the material to induce cell alignment. Further exemplificative images of samples presenting a liquid crystal-induced alignment are reported in Figure S7.

Although, in many cases the use of micropatterned surfaces [35] or nanoconfined environments [30] leads to higher control on cell alignment (with order parameter approaching 1) than those here reported,[35] the use of such smooth film could represent a step towards the upscaling of aligned cell culture due to the simple material preparation and upscaling. The proposed alignment strategy does not require any lithographic technique to structure the substrate, opening to scaffolds that can reach the centimeter scale. Further scaling up of the material seems also feasible as demonstrated by recent studies on the preparation of aligned liquid crystalline network coating by blade or spray techniques.[36] Additional studies will be conducted to investigate if chemical materials modifications (also modifying the LC molecular structures, rather than the ratio between the components) could lead to a further degree of control in cell morphogenesis towards replication *in vitro* of entire pieces of muscles after cell differentiation.

3. Conclusions

A simple method to control the unidirectional alignment in a muscular cell culture is introduced by using a smooth polymeric film. In particular, we tested different liquid crystalline polymeric films presenting various molecular arrangements, created by simply changing the coating in contact with the LC monomeric mixture before the polymerization. C2C12 cells cultured on such substrates demonstrate how it is possible to obtain a unidirectional alignment of the global culture, in contrast to other smooth supports (such as the widely employed Petri dishes).

Such effect is strictly connected to the molecular alignment inside the material and results in a C2C12 anisotropic organization for samples with planar homogeneous alignment, with the prevalent cell orientation direction matching that of the nematic director. These experiments demonstrate for the first time that the liquid crystalline order can be used to manipulate cell growth transferring an information contained inside the polymer at molecular level (the nematic director) to a cell culture.

Moreover, playing only on the monomer composition, e.g. by using higher amount of crosslinker, it is possible to enhance the degree of cellular organization. In contrast to other substrates previously described to align myoblast cultures, the scaffold does not present any particular micro- or nano- patterning, opening to further scale up of the technique thanks to the easy and reliable fabrication method employed. This study opens to a new and simple methodology towards the control of the *in vitro* tissue morphogenesis. To this purpose, it is necessary to better elucidate the relationship between polymer composition and cellular alignment, aiming to extend the liquid crystal-induced alignment mechanism to other cell lines (e.g. cardiomyocyte) and to obtain highly aligned cultures with simple substrates.

4. Experimental Section

LCN fabrication: The monomeric mixture was prepared by mixing monomers **1** (79% or 59% mol/mol), **2** (20% or 40% mol/mol) and Irgacure 396 (**3**, 1% mol/mol) (Figure 2). Mesogens **1** and **2** were purchased by Synthon Chemical, the photoinitiator was purchased from Sigma Aldrich. The mixture was melted at 65 °C on a hot plate and subsequently infiltrated in appropriate polymerization cells by capillarity. The samples prepared in liquid crystalline phase were cooled down until 45 °C (to reach the desired alignment) and irradiated for 10 minutes with an UV LED lamp (Thorlabs M385L2-C4, 385 nm, I= 1.8 mW cm^{-2}). At the end, the LC cells were irradiated for further 10 minutes at 65 °C, immersed in water for 5 minutes (to dissolve the PVA layers) and manually opened with a blade to remove the resulting films.

Samples prepared in isotropic phases were polymerized directly at 90 °C after the infiltration step. Liquid crystalline cells are composed by two coated glass slides using 20 µm sized spheres as spacers. In particular, glasses coated with polyimide PI1211 (Nissan Chemical Industries) were used to obtain the homeotropic LC alignment, while coating with PVA solution was used to induce a planar molecular orientation. The two PVA-coated glasses were rubbed unidirectionally with a velvet cloth before cell assembly to obtain a homogeneous planar alignment.

Film morphology: The morphological characterization of the films was carried out by means of Field Emission-Scanning Electron Microscopy (FE-SEM) and Atomic Force Microscopy (AFM). FE-SEM investigation was performed on gold sputter-coated films (Auto Sputter coater, Agar Scientific), with a Zeiss, Σigma microscope operating at 2kV. AFM was performed on pristine films in non-contact mode with a Park System XE-7 microscope equipped with NCHR probes (radius of curvature about 5 nm). Topography images (resolution 512 x 512 pixels) were acquired by means of the XEP software (version 1.8.4) and corrected for tilting through the flattening function in the XEI software (version 4.1.0, both by Park Systems). Roughness values were calculated as the root-mean-squared roughness (*i.e.*

the standard deviation of the height value) over five different images (each 20 µm x 20 µm) and the data are reported in the paper as mean value ± standard deviation.

Film wettability: Wettability of films was evaluated by measuring the advancing and receding contact angles of pristine films immersed in MilliQ water at 25 ºC, with a K100 Force Tensiometer, Krüss GmbH. Film were immersed/withdrawn during 6 consecutive cycles, with a speed of 3 mm/min, minimum and maximum immersion depths of 1 mm and 5 mm, respectively. Contact angle values were estimated through the Krüss Laboratory Desktop software, version 3.2, as the results of a linear regression of the force *vs* position graph. The regression was carried out in the linear region of the graph for each cycle (both advancing and receding), taking into account width and thickness of films. Data are reported as mean value ± standard deviation over all the cycles, excluding the first one.

Biological assay: LCN films were cut in rectangular stripes (10 x 3mm) with longer side corresponding to the rubbing direction when present. The samples were sterilized and placed in 35 mm Petri dishes. Then, C2C12 murine myoblasts were directly seeded on the samples (a 50 µL drop of medium containing about 25,000 cells is deposited on each LCN stripe) and after 3 hours, cell adhesion was checked by optical microscopy which revealed a confluence lower than 10%. The samples were stored in Dulbecco's modified Eagle's medium (DMEM) with 10% Fetal Bovine Serum (FBS), glutamine, penicillin, streptomycin and, after incubation at 37°C (5% CO_2) for different times, LCNs were washed with PBS and stained using Diff-Quik Kit (Biomap, Italy). The presence of C2C12 adherent cells was evaluated using an optical microscope.

Statistical analysis: The statistical analysis was performed as described in this section and depicted in Figure S1. Firstly, each image was converted to a binary mask highlighting the cell nuclei using a common segmentation pipeline[37]. This image was then fed to a MATLAB script based on the `regionprops` function, to identify each connected region and extract its

properties. Misrecognized regions (Fig. S1b, magenta) were rejected based on their Area value (if smaller than a certain threshold) and on their Area/Convex Area ratio (sometimes referred to as the Solidity), to avoid regions with strange, elongated or hollow shapes typically resulting from damaged or adjacent cell nuclei. In our case, we used 20 pixels and 70% as the lower thresholds for the Area and the Solidity, respectively. Nonetheless, it was found that the final result is largely insensitive to the particular values used for these thresholds, due to the large statistical ensemble used (typically 5-6 wide field images containing a total of ~10^4 nuclei for each sample type, see Figure S2). Our MATLAB script returns an ellipse-based representation of each nucleus (final panel of Figure S1), whose orientation is estimated based on its major axis alignment. This procedure is repeated for a set of optical images obtained at different positions of 3 different sample realizations of each sample type. The final order parameter S for each sample type is obtained as an ensemble average of the orientation angle of all segmented nuclei, with an uncertainty calculated as the standard deviation over the set of S values obtained from single images, typically containing ~1800-2000 nuclei each.

Supporting Information
Supporting Information is available from the Wiley Online Library or from the author.

Acknowledgements
CSGI is acknowledged for financially supporting the physical-chemical characterization activities. The research leading to these results has also received funding from Laserlab-Europe EU-H2020 654148 and from Ente Cassa di Risparmio di Firenze (grant 2015/0781), Fondazione Telethon (grant GGP16191).

Received: ((will be filled in by the editorial staff))
Revised: ((will be filled in by the editorial staff))
Published online: ((will be filled in by the editorial staff))

References

[1] M. B. Chan-Park, J. Y. Shen, Y. Cao, Y. Xiong, Y. Liu, S. Rayatpisheh, G. C.-W. Kang, H. P. Greisler, *J. Biomed. Mater. Res. Part A* **2009**, *88*, 1104.

[2] E. M. Bartels, B. Danneskiold-Samsoe, *Lancet* **1986**, *327*, 755.

[3] J. Zhang, W. Zhu, M. Radisic, G. Vunjak-Novakovic, *Circ. Res*. **2018**, *123*, 244.

[4] Y. Li, G. Huang, X. Zhang, L. Wang, Y. Du, T. J. Lu, F. Xu, *Biotech. Adv.* **2014**, 32, 347.

[5] M. Nikkhah, F. Edalat, S. Manoucheri, A. Khademhosseini, *Biomaterials* **2012**, *33*, 5230.

[6] T. B. Saw, W. Xi, B. Ladoux, C. T. Lim, *Adv. Mater.* **2018**, 1802579.

[7] G. Duclos, S. Garcia, H. G. Yevick, P. Silberzan, *Soft Matter* **2014**, *10*, 2346.

[8] T. B. Saw, A. Doostmohammadi, V. Nier, L. Kocgozlu, S. Thampi, Y. Toyama, P. Marcq, C. T. Lim, J. M. Yeomans, B. Ladoux, *Nature* **2017**, *544*, 212.

[9] C. Peng, T. Turiv, Y. Guo, Q. H. Wei, O. D. Lavrentovich, *Science* **2016**, 354, 882.

[10] A. Agarwal, E. Huang, S. Palecek, N. L. Abbott, *Adv. Mater*. **2008**, *20*, 4804.

[11] D. Martella, C. Parmeggiani, *Chem. Eur. J.* **2018**, *24*, 12206.

[12] T. J. White, D. J. Broer, *Nat. Mater.* **2015**, *14*, 1087.

[13] C. Ohm, M. Brehmer, R. Zentel, *Adv. Mater.* **2010**, *22*, 3366.

[14] P. G. De Gennes, M. Hébert, R. Kant, *Macromol. Symp.* **1997**, *113*, 39.

[15] a) M. Yamada, M. Kondo, J. I. Mamiya, Y. Yu, M. Kinoshita, C. J. Barrett, T. Ikeda, *Angew. Chem.* **2008**, *120*, 5064; b) D. Martella, S. Nocentini, D. Nuzhdin, C. Parmeggiani, D. S. Wiersma, *Adv. Mater.* **2017**, *29*, 1704047; c) S. Nocentini, C. Parmeggiani, D. Martella, D. S. Wiersma, *Adv. Optical Mater.* **2018**, 6, 1800207.

[16] a) S. Nocentini, D. Martella, C. Parmeggiani, S. Zanotto, D. S. Wiersma, *Adv. Opt. Mater.* **2018**, *6*, 1800167; b) S. Nocentini, F. Riboli, M. Burresi, D. Martella, C. Parmeggiani, D. S. Wiersma, *ACS Photonics* **2018**, *5*, 3222.

[17] M. E. Prévôt, H. Andro, S. L. M. Alexander, S. Ustunel, C. Zhu, Z. Nikolov, S. T. Rafferty, M. T. Brannum, B. Kinsel, L. T. J. Korley, E. J. Freeman, J. A. McDonough, R. J. Clements, E. Hegmann, *Soft Matter* **2018**, *14*, 354.

[18] A. Agrawal, H. Chen, H. Kim, B. Zhu, O. Adetiba, A. Miranda, A. C. Chipara, P. M. Ajayan, J. G. Jacot, R. Verduzco, *ACS Macro Lett.* **2016**, *5*, 1386.

[19] Y. Gao, T. Mori, S. Manning, Y. Zhao, A. D. Nielsen, A. Neshat, A. Sharma, C. J. Mahnen, H. R. Everson, S. Crotty, R. J Clements, C. Malcuit, E. Hegmann, *ACS Macro Lett.* **2015**, *5*, 4.

[20] D. Martella, P. Paoli, J. M. Pioner, L. Sacconi, R. Coppini, L. Santini, M. Lulli, E. Cerbai, D. S. Wiersma, C. Poggesi, C. Ferrantini, C. Parmeggiani, *Small* **2017**, *13*, 1702677.

[21] G. Koçer, J. ter Schiphorst, M. Hendrikx, H. G. Kassa, P. Leclère, A. P. Schenning, P. Jonkheijm, *Adv. Mater.* **2017**, *29*, 1606407.

[22] S. Burattini, P. Ferri, M. Battistelli, R. Curci, F. Luchetti, E. Falcieri, *Eur. J. Histochem.* **2009**, *48*, 223.

[23] N. F. Huang, S. Patel, R. G. Thakar, J. Wu, B. S. Hsiao, B. Chu, R. J. lee, S. Li, *Nano Lett.* **2006**, *6*, 537.

[24] D. Liu, D. J. Broer, *Langmuir* **2014**, *30*, 13499.

[25] D. Martella, D. Antonioli, S. Nocentini, D. S. Wiersma, G. Galli, M. Laus, C. Parmeggiani, *RSC Adv.* **2017**, *7*, 19940.

[26] S. Nocentini, D. Martella, C. Parmeggiani, D. S. Wiersma, *Materials* **2016**, *9*, 525.

[27] P. G. de Gennes, J. Proust, *The physics of liquid crystals- 2nd Edition*, Oxford University Press, Oxford, UK, **2003**.

[28] A. Umeno, H. Kotani, M. Iwasaka, S. Ueno, *IEEE Trans. Magn.* **2001**, *37*, 2909.

[29] J. L. Charest, A. J. García, W. P. King, *Biomaterials* **2007**, *28*, 2202.

[30] X. Li, R. Balagam, T. F. He, P. P. Lee, O. A. Igoshin, H. Levine, *Proc. Natl. Ac. Sci.* **2017**, *114*, 8974.

[31] H. Aubin, J. W. Nichol, C. B. Hutson, H. Bae, A. L. Sieminski, D. M. Cropek, P. Akhyari, A. Khademhosseini, *Biomaterials* **2010**, *31*, 6941.

[32] E. Rebollar, I. Frischauf, M. Olbrich, T. Peterbauer, S. Hering, J. Preiner, P. Hinterdorfer, C. Romanin, J. Heitz, *Biomaterials* **2008**, *29*, 1796.

[33] R. A. M. Hikmet, D. J. Broer, *Polymer* **1991**, *32*, 1627.

[34] Y. Sawa, F. Ye, K. Urayama, T. Takigawa, V. Gimenez-Pinto, R. L. Selinger, J. V. Selinger, *Proc. Natl. Acad. Sci.* **2011**, *108*, 6364.

[35] D. H. Kim, E. A. Lipke, P. Kim, R. Cheong, S. Thompson, M. Delannoy, K. Y. Suh, L. Tung, A. Levchenko, *Proc. Natl. Acad. Sci.* **2010**, *107*, 565.

[36] R. C. Verpaalen, M. G. Debije, C. W. Bastiaansen, H. Halilović, T. A. Engels, A. P. Schenning, *J. Mater. Chem. A*, **2018**, *6*, 17724.

[37] C. Sommer, C. Strähle, U. Köthe, F. A. Hamprecht. In: *Eighth IEEE International Symposium on Biomedical Imaging (ISBI): Proceedings*, **2011**, 230-233.